



THE UNIVERSITY *of* EDINBURGH

Edinburgh Research Explorer

Chemical Modulation of in vivo Macrophage Function with Subpopulation-Specific Fluorescent Prodrug Conjugates

Citation for published version:

Fernandez Vargas, A, Vermeren, M, Humphries, D, Subiros Funosas, R, Barth, N, Campana, L, MacKinnon, A, Feng, Y & Vendrell Escobar, M 2017, 'Chemical Modulation of in vivo Macrophage Function with Subpopulation-Specific Fluorescent Prodrug Conjugates' ACS central science, vol. 3, no. 9, pp. 995-1005. DOI: 10.1021/acscentsci.7b00262

Digital Object Identifier (DOI):

[10.1021/acscentsci.7b00262](https://doi.org/10.1021/acscentsci.7b00262)

Link:

[Link to publication record in Edinburgh Research Explorer](#)

Document Version:

Publisher's PDF, also known as Version of record

Published In:

ACS central science

Publisher Rights Statement:

This is an open access article published under a Creative Commons Attribution (CC-BY) License, which permits unrestricted use, distribution and reproduction in any medium, provided the author and source are cited.

General rights


Copyright for the publications made accessible via the Edinburgh Research Explorer is retained by the author(s) and / or other copyright owners and it is a condition of accessing these publications that users recognise and abide by the legal requirements associated with these rights.

Take down policy

The University of Edinburgh has made every reasonable effort to ensure that Edinburgh Research Explorer content complies with UK legislation. If you believe that the public display of this file breaches copyright please contact openaccess@ed.ac.uk providing details, and we will remove access to the work immediately and investigate your claim.



Chemical Modulation of *in Vivo* Macrophage Function with Subpopulation-Specific Fluorescent Prodrug Conjugates

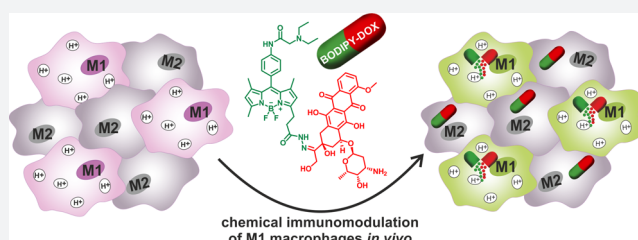
Antonio Fernandez,[†] Matthieu Vermeren,[†] Duncan Humphries,[†] Ramon Subiros-Funosas,[†] Nicole Barth,[†] Lara Campana,[‡] Alison MacKinnon,[†] Yi Feng,^{*,†} and Marc Vendrell^{*,†} 

[†]MRC/UoE Centre for Inflammation Research, Queen's Medical Research Institute, The University of Edinburgh, 47 Little France Crescent, EH16 4TJ Edinburgh, United Kingdom

[‡]MRC Centre for Regenerative Medicine, SCRM Building, The University of Edinburgh, 5 Little France Drive, Edinburgh EH16 4UU, United Kingdom

Supporting Information

ABSTRACT: Immunomodulatory agents represent one of the most promising strategies for enhancing tissue regeneration without the side effects of traditional drug-based therapies. Tissue repair depends largely on macrophages, making them ideal targets for proregenerative therapies. However, given the multiple roles of macrophages in tissue homeostasis, small molecule drugs must be only active in very specific subpopulations. In this work, we have developed the first prodrug–fluorophore conjugates able to discriminate closely related subpopulations of macrophages (i.e., proinflammatory M1 vs anti-inflammatory M2 macrophages), and employed them to deplete M1 macrophages *in vivo* without affecting other cell populations. Selective intracellular activation and drug release enabled simultaneous fluorescence cell tracking and ablation of M1 macrophages *in vivo*, with the concomitant rescue of a proregenerative phenotype. *Ex vivo* assays in human monocyte-derived macrophages validate the translational potential of this novel platform to develop chemical immunomodulatory agents as targeted therapies for immune-related diseases.



INTRODUCTION

The regenerative capacity of organisms is largely influenced by the local immune response to tissue damage, with macrophages being a central component.¹ Macrophages are multifunctional phagocytic cells, which play a pivotal role in the repair of most tissues² and exhibit different phenotypes depending on their microenvironment.³ Conventionally, macrophages are categorized into proinflammatory M1 and tissue-repairing M2 phenotypes.⁴ Tissue regeneration depends largely on macrophages, making them promising targets for proregenerative immunomodulatory therapies.⁵ However, given the plasticity and multiple roles of macrophages in tissue homeostasis, it is essential that macrophage-targeting therapies deplete only specific subpopulations. Whereas this can be partially achieved by genetic methods in transgenic models,⁶ there are no chemical agents that can be clinically translated which can effectively target subpopulations of macrophages *in vivo* and modulate tissue regeneration.

Our group and others have developed chemical tools to examine macrophage activity *in vivo*.^{7–10} The groups of Schultz and Bogoy described Förster resonance energy transfer (FRET) probes to monitor the enzymatic activity of macrophages in pulmonary inflammation (e.g., matrix metalloproteinase 12, MMP12)¹¹ and cancer (e.g., cathepsins in tumor-associated macrophages), respectively.^{12–14} Chang and co-workers recently reported near-infrared fluorophores with preferential uptake in macrophages and enhanced spectral properties for *in*

in vivo imaging.^{15,16} These imaging probes provide generic readouts of macrophage activity but cannot modulate their function *in vivo*.

Prodrug–fluorophore conjugates have been described as effective tools to deliver fluorescent and therapeutic loads into target cells with enhanced selectivity and reduced side effects.¹⁷ Most conjugates have been reported in the context of cancer therapy, either for photodynamic cell ablation¹⁸ or for fluorescence-guided removal of tumor cells,^{19,20} as healthy and cancer cells can be readily discriminated by several biomarkers. In the context of immune modulation, very few prodrugs have been reported to activate in subsets of immune cells. Blum *et al.* described cathepsin-regulated theranostic photosensitizers to ablate macrophages in aggressive breast cancer mouse models and in atherosclerotic plaques.^{21,22} To the best of our knowledge, there are no prodrug–fluorophore conjugates that can monitor and modulate the function of M1 macrophages *in vivo*.

The 4,4-difluoro-4-bora-3a,4a-diaza-*s*-indacene (BODIPY) scaffold has been widely used in the development of fluorescent probes due to its excellent photophysical and cell permeability properties.^{23–27} Our group has demonstrated the suitability of BODIPY fluorophores for imaging phagosomal acidification in macrophages in real time.²⁸ Given the phagosomal pH and

Received: June 19, 2017

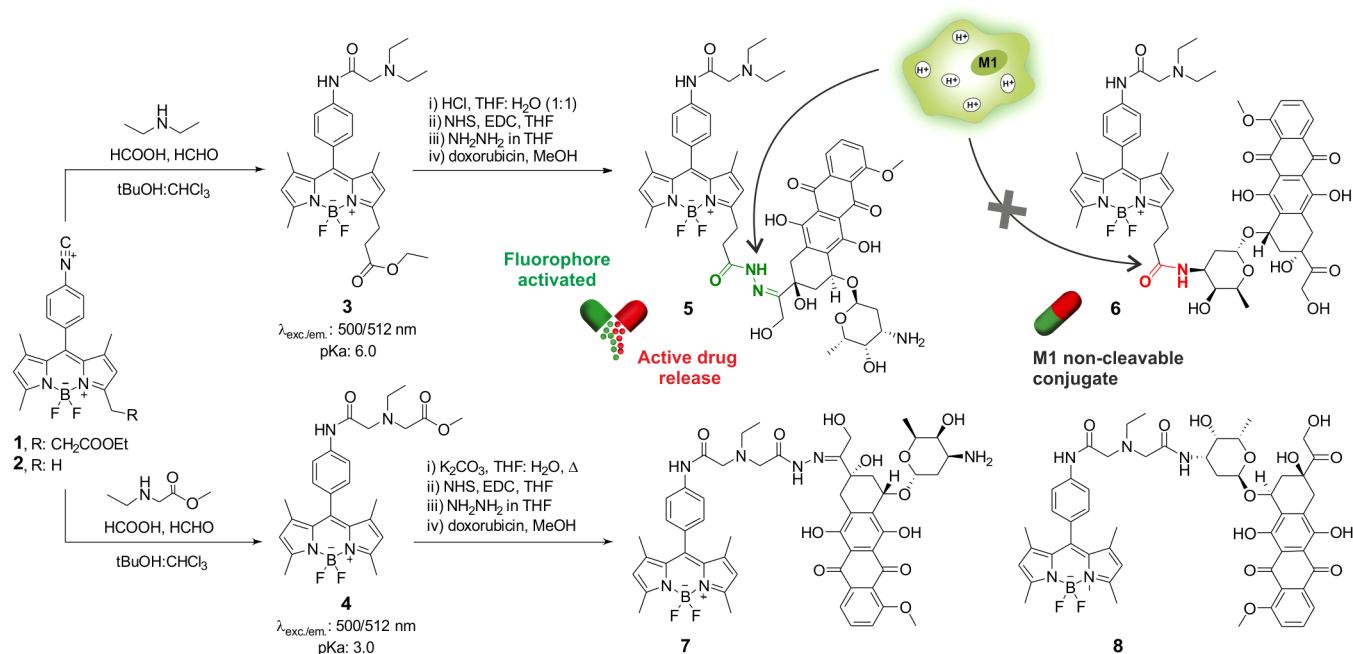


Figure 1. Synthesis of fluorogenic BODIPY–prodrug M1 activatable conjugates.

hydrolytic activity of M1 murine macrophages,²⁹ we envisaged that prodrug–fluorophore conjugates targeting acidic phagosomes would allow us to reprogram the immune function of M1 macrophages with high precision and marginal side effects while tracking the fate of drug-treated macrophages *in vivo*. Herein we have developed BODIPY–prodrug conjugates targeting M1 macrophages with negligible effects in other macrophage subpopulations. The specific release of BODIPY activatable fluorophores and cytotoxic drugs into M1 macrophages enabled blocking of the proinflammatory macrophage phenotype *in vivo* in a model of tissue regeneration. Besides, the translational potential of these novel conjugates in human macrophages opens multiple avenues in precision medicine for the chemical modulation of immune cell function.

RESULTS AND DISCUSSION

Synthesis and Characterization of Fluorescent Prodrug Activatable Conjugates for M1 Macrophages.

Activatable prodrugs have been widely described in the literature as enhanced delivery molecules to improve therapeutic efficacy in target cells while reducing potential side effects in off-target cells.^{30,31} For instance, glutathione-activatable prodrugs have been successfully developed as theranostic agents with enhanced cytotoxic activity in cancer cells.^{32,33} Similar chemical strategies have been also used in the construction of smart nanomaterials with increased response-to-noise ratios in specific tissues.^{34,35} Among the different subpopulations of macrophages, M1 macrophages contain intracellular acidic phagosomes. Acidic phagosomes present pH values between 4.5 (late phagosomes) and 6.5 (early phagosomes), depending on their maturation state.^{36,37} We envisioned that the conjugation of cytotoxic drugs to pH-activatable BODIPY fluorophores through phagosome-cleavable spacers would allow us to specifically deplete the proinflammatory activity of M1 macrophages. In order to construct BODIPY–prodrug conjugates that would be specifically cleaved in M1 macrophages but not in other macrophages, we synthesized the core scaffold of a pH-

activatable fluorophore including two ester spacers at different positions of the BODIPY structure (3 and 4, Figure 1). Compounds 3 and 4 were obtained in good yields by derivatization of their corresponding isonitriles 1 and 2 via Ugi multicomponent reaction at the *meso* position of the BODIPY scaffold with diethylamine and methyl *N*-ethylglycinate, respectively (Figure 1).

The key intermediates in the synthesis of 1 and 2 were their corresponding BODIPY nitro derivatives [see the Supporting Information for full synthetic and characterization details], which were hydrogenated, formylated with ethyl formate, and dehydrated with POCl_3 to render the corresponding pH-insensitive BODIPY isonitriles (1 and 2). First, we evaluated the fluorescence properties of the esters 3 and 4 at different pH values in order to assess their suitability to monitor phagosomal acidification in M1 macrophages. The two BODIPY esters (3 and 4) exhibited pH-dependent fluorescence emission, however very divergent pK_a values (Figure 2A and Figure S5). Compound 3 showed a pK_a of 6.0 as well as strong fluorescence staining in lipopolysaccharide (LPS)-stimulated M1 macrophages but not in nonactivated macrophages (Figures 2C and 2D). On the other hand, compound 4 (pK_a : 3.2) and the pH-insensitive isonitrile 2 were unable to label M1 macrophages. These results point at the diethylamine group in compound 3 as the key structural feature to achieve pH sensitivity in the appropriate range for M1 macrophage sensing (i.e., between 4.5 and 6.5). The dissimilar behavior of compound 4 suggests that any modifications in the diethylamine group might alter not only the pH-dependent fluorescence response but also the acidotropic accumulation of BODIPY fluorophores in macrophages.

In view of these results, we derivatized compound 3 with an acid-cleavable *N*-acylhydrazone group for controlled release of both fluorescent and therapeutic molecules in the acidic phagosomes of M1 macrophages.³⁸ In order to target and block the proinflammatory function of M1 macrophages, we conjugated the profluorophore 3 to doxorubicin as a cytotoxic molecule for M1 macrophage depletion.³⁹ We envisaged that

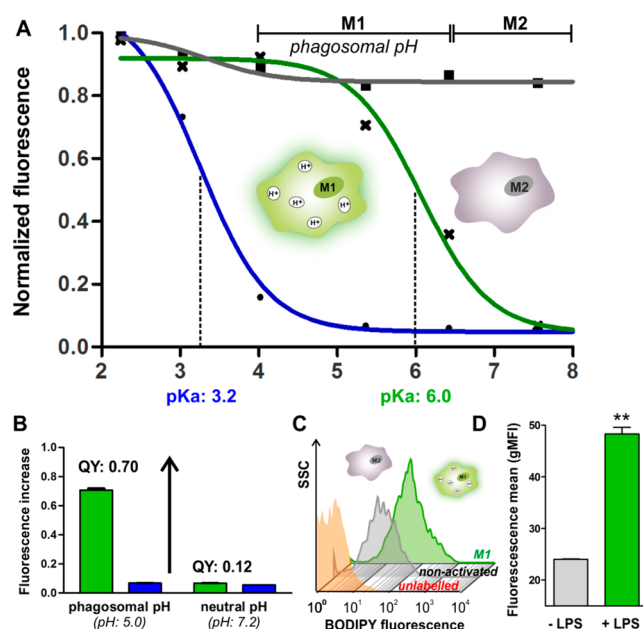


Figure 2. Comparative fluorescence staining of M1 macrophages using BODIPY derivatives. (A) Fluorescence intensity of compounds 2 (square, gray), 3 (cross, green), and 4 (circle, blue) at different pH values. (B) Fluorescence fold increase of compounds 3 (green, 15 μM) and 4 (blue, 15 μM) between phagosomal and neutral pH. (C, D) Flow cytometry analysis of LPS-induced M1 macrophages (LPS: 100 ng mL^{-1} , 18 h) and nontreated macrophages after incubation with compound 3 (10 μM). SSC: side cell scattering. QY: fluorescence quantum yield. Values represented as means \pm SD. ($n = 4$). ** for $p < 0.01$.

the phagosomal pH would accelerate the cleavage of the *N*-acylhydrazone group to activate both fluorescent and functional responses in M1 macrophages. We prepared the BODIPY–doxorubicin hydrazone 5 by hydrolysis of the ethyl ester 3 in acidic conditions, followed by one-pot hydrazone formation via activation as succinidimyl ester and reaction with hydrazine in THF. The conjugation of the hydrazone to the carbonyl group of doxorubicin was performed in MeOH using catalytic amounts of trifluoroacetic acid to render compound 5 as an activatable BODIPY–prodrug with a pH-labile linker (Figure 1). The nonlabile BODIPY–doxorubicin amide conjugate 6 was also prepared as a negative control. In this case, activation of compound 3 with (1-cyano-2-ethoxy-2-oxoethylideneaminoxy)-dimethylamino-morpholino-carbenium hexafluorophosphate (COMU) and DIPEA in DMF, followed by conjugation to the amine group of doxorubicin, yielded the amide derivative 6. Furthermore, hydrazone and amide BODIPY–doxorubicin conjugates of the ester 4 (compounds 7 and 8, respectively) were also prepared as additional negative controls of BODIPY–prodrug conjugates including labile groups not matching the phagosomal pH in M1 macrophages (Figure 1). Notably, the spectral characterization of all derivatives showed that excitation and emission wavelengths of the conjugates remained unaltered after conjugation to doxorubicin (Table S1 and Figure S7), with the BODIPY core being the main contributor to the fluorescence emission (Figure S8).

Functional Assays in M1 and M2 Macrophage Subpopulations. First, we evaluated the suitability of the BODIPY–doxorubicin conjugates as efficient prodrugs for macrophages. We compared the cell viability of nonactivated RAW264.7 murine macrophages after treatment with doxor-

ubicin alone and with the conjugates 5–8 (Figure S6). Whereas doxorubicin induced significant dose-dependent cell toxicity, none of the BODIPY conjugates showed any effects in the cell viability of macrophages, indicating that the cytotoxic action of doxorubicin was effectively blocked via derivatization with *N*-acylhydrazone (5, 7) or amide (6, 8) groups. Furthermore, we also confirmed that the BODIPY fluorophores on their own (compounds 3 and 4) did not induce any cytotoxicity in macrophages (Figure S6).

Next, we assessed the functional effects of compound 5 in separate M1 and M2 macrophage subpopulations. We employed reported protocols to activate macrophage cells toward classical M1 (treatment with LPS) or alternative M2 phenotypes (treatment with IL-4) and incubated them with different concentrations of compound 5. As shown in Figure 3A, the phagosomal acidification in M1 macrophages enabled

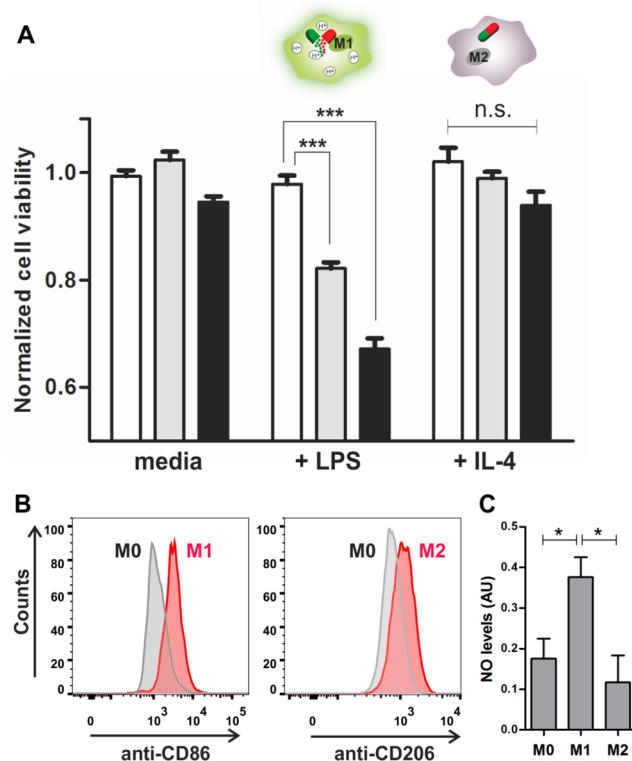


Figure 3. Functional assays in M1 and M2 mouse macrophages. (A) Incubation of compounds 6 (10 μM , white) and 5 (5 μM , gray; 10 μM , black) in different subpopulations of macrophages confirm a dose-dependent release of doxorubicin (determined by cell viability) from 5 in M1 macrophages. (B) Flow cytometry histograms of LPS-induced (100 ng mL^{-1} , 18 h) M1 macrophages and IL-4-induced (100 ng mL^{-1} , 18 h) M2 macrophages vs nontreated macrophages (M0) after incubation with anti-CD86-APC (M1 marker, 2 $\mu\text{g mL}^{-1}$) or anti-CD206-APC (M2 marker, 2 $\mu\text{g mL}^{-1}$). (C) NO production assay in cell supernatants from nontreated, M1, and M2 macrophages. Values represented as means \pm SD ($n = 4$). n.s. for $p > 0.05$, * for $p < 0.05$, ** for $p < 0.01$, *** for $p < 0.001$.

the release of the cytotoxic doxorubicin in a dose-dependent manner, whereas no functional effects were observed in either quiescent or M2 macrophages. Polarization of macrophages toward M1 or M2 phenotypes was confirmed by expression of cell-surface markers in flow cytometry analysis (i.e., CD86 for M1 macrophages,⁴⁰ CD206 in M2 macrophages⁴¹) (Figure 3B) and nitric oxide (NO) production⁴² (Figure 3C). Notably,

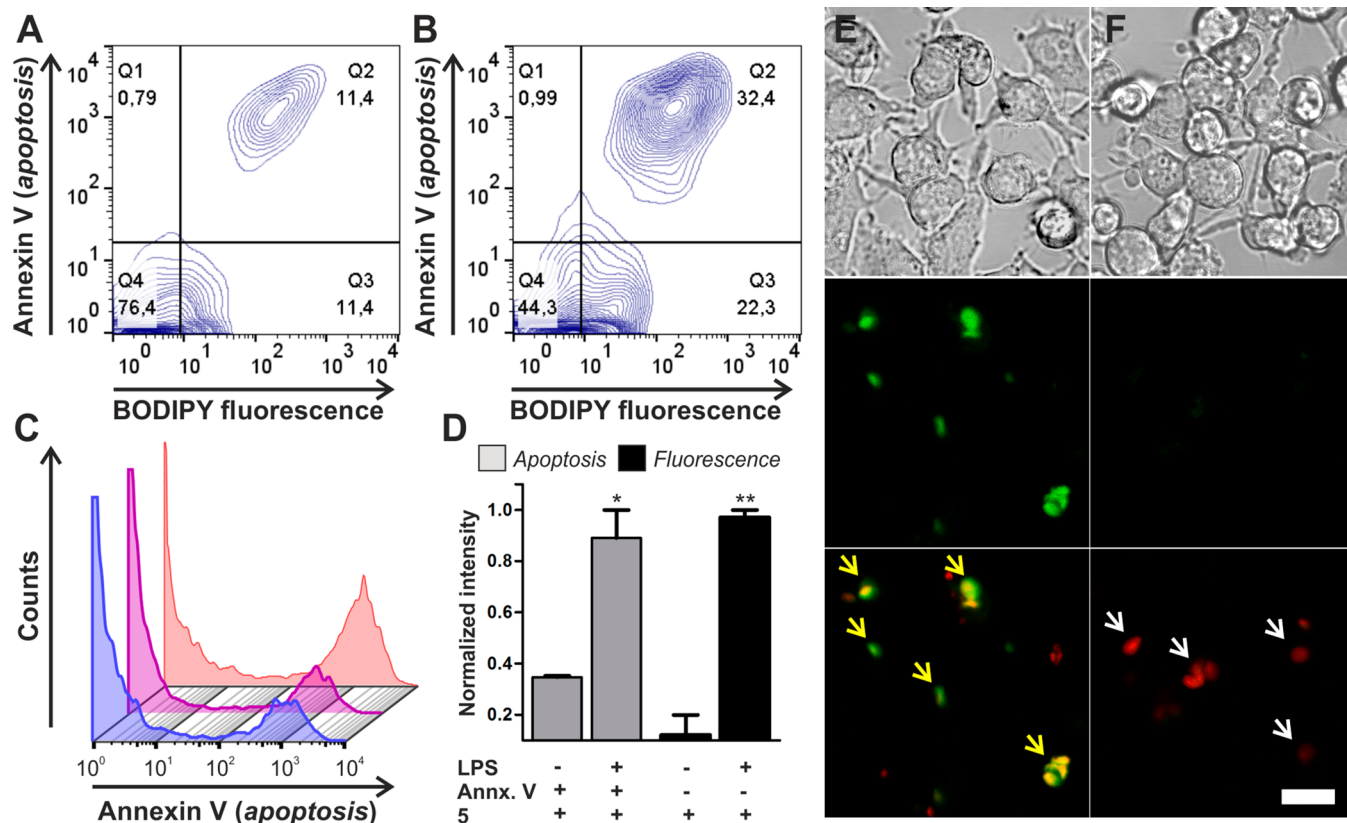


Figure 4. Flow cytometry analysis after treatment with compound **5** ($10\ \mu\text{M}$) and Annexin V-AF647 (1:100) in (A) nonactivated mouse macrophages and (B) LPS-induced ($100\ \text{ng mL}^{-1}$, 18 h) M1 mouse macrophages. (C) Histograms showing Annexin V-AF647 staining in mouse macrophages that were treated with LPS ($100\ \text{ng mL}^{-1}$, 18 h) (blue), compound **5** ($10\ \mu\text{M}$) (purple), and combined LPS ($100\ \text{ng mL}^{-1}$, 18 h) and compound **5** ($10\ \mu\text{M}$) (red). (D) Normalized quantification of fluorescence intensities for Annexin V-AF647 (gray) and BODIPY fluorescence (black). Values represented as means \pm SD ($n = 3$). * for $p < 0.05$, ** for $p < 0.01$. (E) Fluorescence confocal microscopy of live macrophages upon treatment with green-fluorescent BODIPY hydrazone **5** ($150\ \text{nM}$) and red-fluorescent (Texas Red) zymosan beads ($0.05\ \text{mg mL}^{-1}$, 1 h). Brightfield (top), green fluorescence (center), and merged green-red fluorescence (bottom) images of macrophages without (E) or with bafilomycin A ($100\ \text{nM}$, 1 h) preincubation (F). Yellow arrows (in E) and white arrows (in F) point at zymosan-uptaking M1 macrophages. Scale bar: $10\ \mu\text{m}$.

incubation of M1 and M2 macrophage subpopulations with the noncleavable amide derivative **6** did not cause any cytotoxicity, indicating the phagosomal pH-induced cleavage as the primary mechanism for the specific release of doxorubicin in M1 macrophages (Figure S9). HPLC–MS analysis of the acid-cleavable hydrazone **5** confirmed the cleavage of doxorubicin only under acidic environments, with no drug release observed at neutral pH or for the noncleavable amide conjugate **6** (Figure S10). We further characterized the functional effects of the hydrazone **5** in M1 macrophages by immunochemical analysis (Figure S11). In these assays, we measured the levels of several cytokines in LPS-stimulated M1 macrophages that had been treated or not with hydrazone **5** and observed a reduction in the production of key cytokines and chemokines (e.g., TNF- α) associated with the M1 macrophage phenotype. In addition, we corroborated that IL-4-stimulated macrophages presented increased arginase activity as a result of their M2 polarization⁴³ (Figure S12).

Fluorescence Analysis of M1 Macrophages. Prodrug–fluorophore conjugates are advantageous in that they enable monitoring cell fate upon drug release using fluorescence readouts.⁴⁴ As such, we compared the fluorescence staining of nonactivated macrophages and M1 macrophages after incubation with compound **5** by flow cytometry. Nonactivated macrophages displayed low BODIPY fluorescence staining (Figure 4A), while strong fluorescence emission was observed

in LPS-stimulated M1 macrophages (Figure 4B), indicating the efficient cell uptake of compound **5** and its intracellular activation upon phagosomal acidification. Furthermore, we compared the apoptotic index of both macrophage subpopulations by coinubation with Annexin V as a direct functional readout of cellular apoptosis due to doxorubicin release inside macrophages. The low apoptotic index in nonactivated macrophages increased 3-fold in LPS- and **5**-treated M1 macrophages (Figure 4C). Moreover, apoptotic cells (i.e., Annexin V stained cells) displayed also strong BODIPY fluorescence (Figure 4B), confirming the simultaneous release of doxorubicin and the BODIPY fluorophore in M1 macrophages.

Next, in order to assess the subcellular localization of the released cargo in live macrophages, we imaged RAW264.7 macrophages after incubation with compound **5** under fluorescence confocal microscopy. Macrophages were stimulated with zymosan, a glycan isolated from yeast cells that induces classical M1 activation.⁴⁵ Zymosan beads were conjugated to the pH-insensitive fluorophore Texas red so that two-color fluorescence images could be acquired. As shown in Figure 4E, strong colocalization was observed between the green BODIPY fluorophore and red-fluorescent zymosan in the intracellular phagosomes of live macrophages. This observation confirms that M1 macrophages uptaking zymosan beads turn on the pH-activatable BODIPY fluorophore. To confirm this

hypothesis, we preincubated live macrophages with bafilomycin A—an inhibitor of the vacuolar-type H⁺-ATPase required for phagosomal acidification⁴⁶—and then treated them with red zymosan beads and compound 5. The images shown in Figure 4F confirmed that phagosomal acidification was the main intracellular mechanism for the activation of the pH-sensitive BODIPY fluorophore, as bafilomycin-treated M1 macrophages were not green fluorescently stained despite having taken up red zymosan beads. Together with the functional assays, these results assert the potential of compound 5 as an effective prodrug and activatable BODIPY imaging agent to visualize and modulate the function of M1 macrophages.

Subpopulation Discrimination of Macrophages and *ex Vivo* Assays in Human Macrophages. To evaluate the selective activation of compound 5 in mixtures of cells with different phenotypes, we cultured M1 and M2 macrophages in a Transwell assay to coculture both subpopulations with the same concentration of compound 5. RAW264.7 macrophages were plated and polarized toward M1 and M2 populations and then treated for 20 h with compound 5 under physiological conditions. The two subpopulations were exposed to the same experimental conditions, being only separated by a membrane permeable to small molecules (Figure 5A). After incubation, both subpopulations were isolated, treated with Annexin V, and analyzed by flow cytometry. As shown in Figure 5B, M1 macrophages showed around 4-fold higher apoptotic index than M2 macrophages (indicated by Annexin V staining, 72% vs 19%). Annexin V positive cells were also stained with the BODIPY fluorophore, confirming the enhanced hydrolytic activity of M1 over M2 macrophages after 20 h. These results confirm the preferential activation of compound 5 (i.e., doxorubicin intracellular release and fluorescence emission) in M1 macrophages, even in the presence of other macrophage subpopulations.

Whereas *in vivo* cell ablation has been achieved by incorporating genetically encoded receptors (e.g., diphtheria toxin receptor, DTR) into specific cell lineages,⁴⁷ including macrophages, such approaches are poorly translatable to clinical environments. In order to examine the translational potential of compound 5 to deplete subpopulations of human M1 macrophages, we isolated and cultured monocyte-derived macrophages from human peripheral blood. Macrophages were stimulated with LPS and polarized toward the M1 phenotype, which was confirmed by increased expression of the cell-surface marker CD86 (Figures 5C and 5D) and the tumor necrosis factor alpha (TNF- α)⁴⁸ (Figure S13). Under these conditions, human macrophages were treated with both activatable and nonactivatable BODIPY–prodrug conjugates (i.e., compounds 5 and 6, respectively). The incubation of LPS-stimulated human M1 macrophages with compound 5 led to significant enhancement of the fluorescence emission (Figures 5C and 5D) and effective doxorubicin release that resulted in reduced cell viability (Figures 5E and 5F). Flow cytometric analysis confirmed the double-positive staining of human M1 macrophages with a fluorescently labeled anti-CD86 antibody and compound 5 (Figure S14), indicating preferential activation of compound 5 in human M1 macrophages. Furthermore, we also corroborated that the treatment of human M1 macrophages with the noncleavable BODIPY–prodrug 6 did not cause any cytotoxic effect (Figure S15). These results suggest that phagosomal pH is a species-independent activation mechanism to release prodrugs in defined subpopulations of macrophages and also assert the

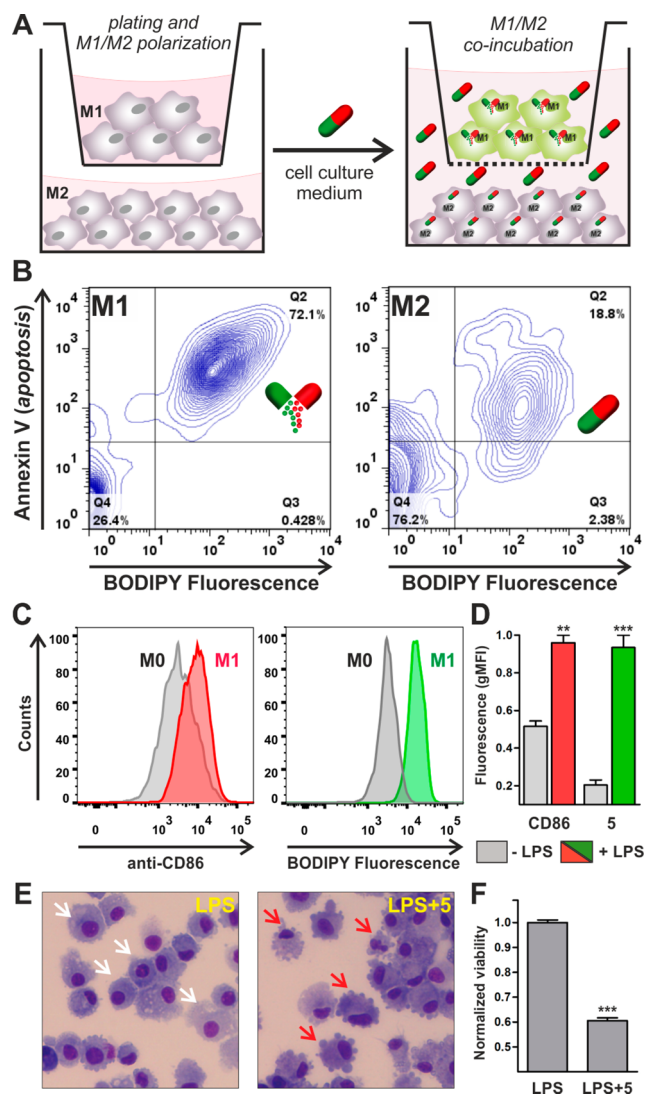


Figure 5. Discrimination of M1/M2 mouse macrophages and *ex vivo* assays in human macrophages. (A) Schematic representation of the Transwell assay with mouse macrophages, where M1 and M2 subpopulations are physically isolated through a membrane permeable to small molecules. (B) Flow cytometry analysis of both M1 and M2 mouse subpopulations after coincubation with compound 5 (10 μ M) under physiological conditions and subsequent costaining with Annexin V. (C, D) Flow cytometry histograms and quantification of LPS-induced (100 ng mL⁻¹, 18 h) human M1 macrophages vs nontreated macrophages (M0) after incubation with anti-CD86-APC (M1 marker, 2 μ g mL⁻¹) and compound 5 (1 μ M). (E) Cytospin analysis of human M1 macrophages after treatment with LPS alone or LPS and compound 5 revealed morphological differences between viable macrophages (white arrows) and preapoptotic nonviable macrophages (red arrows) due to doxorubicin release. (F) Cell viability of human macrophages after M1 polarization (100 ng mL⁻¹ LPS, 18 h) and incubation with compound 5 (10 μ M). Values represented as means \pm SD ($n = 3$). ** for $p < 0.01$, *** for $p < 0.001$.

potential of compound 5 for translational studies in human macrophages.

***In Vivo* Functional and Imaging Assays.** In view of the excellent properties of 5 as a BODIPY–prodrug conjugate to deplete subpopulations of macrophages, we investigated its application to modulate immune cell function in a zebrafish model of tissue regeneration. When their tail fin is amputated at 2 days postfertilization (dpf), zebrafish larvae regenerate their

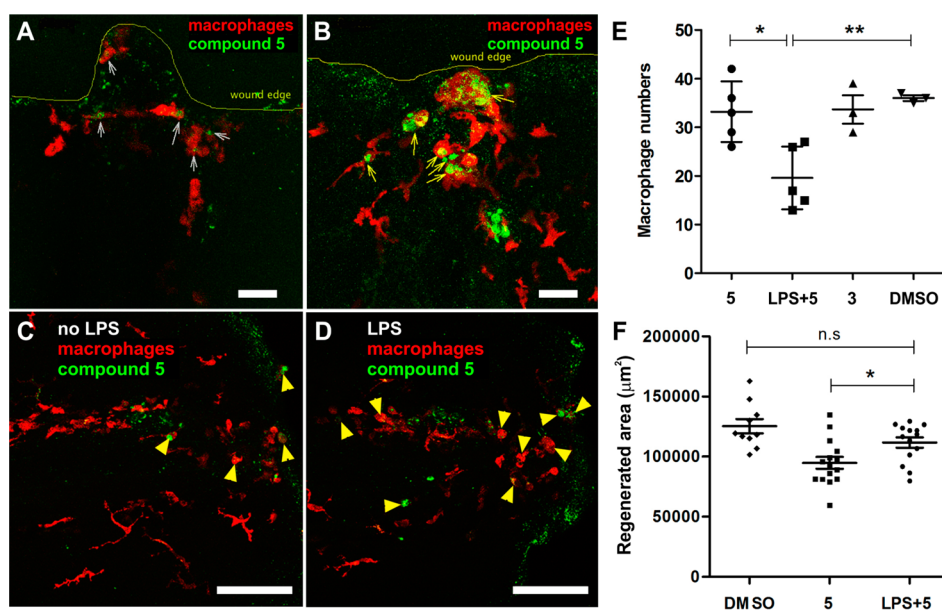


Figure 6. *In vivo* imaging of macrophages in a zebrafish model of tissue regeneration. Snapshot fluorescence microscopy images of macrophages recruited to the wounded edge at 1 hpt (A, [Movie S1](#), white arrows) and 24 hpt (B, [Movie S2](#), yellow arrows). High magnification images of macrophages at the regenerative tail fin of 5-treated zebrafish (3 μM) without (C) and with (D) LPS treatment (100 ng mL⁻¹) at 48 hpt. Yellow arrowheads point at rounded apoptotic and necrotic macrophages upon doxorubicin release. Scale bars: 50 μm . (E) Quantification of macrophage numbers after incubation with DMSO or compounds 3, 5, and LPS. (F) *In vivo* quantitative analysis of the regenerated tissue area. Zebrafish larvae were treated with DMSO or compound 5 with and without LPS pretreatment, and the regeneration area upon tail fin injury was determined at 48 hpt. Values represented as means \pm SD ($n \geq 10$). n.s for $p > 0.05$, * for $p < 0.05$, ** for $p < 0.01$.

fin within 72 h postwounding (hpw). Under these conditions, macrophages migrate toward the amputation site within 1–2 hpw and their number is typically maintained to enable tissue regeneration.⁴⁹ We explored the applicability of compound 5 to visualize recruited macrophages by fluorescence imaging as well as to alter tissue regeneration *in situ* by depleting M1 macrophages *in vivo*. Upon tail fin amputation, we treated zebrafish larvae with compound 5 and performed time-lapse imaging by live fluorescence confocal microscopy. As shown in [Figure 6A](#) and [Movie S1](#), mCherry-expressing macrophages were recruited to the injury site but only a few macrophages showed green fluorescence corresponding to the intracellular activation of compound 5. This is in agreement with reported observations that correlate the initial recruitment of macrophages to injury sites to the M2 wound-healing phenotype and not the M1 proinflammatory phenotype.⁵⁰ Images at longer time points [i.e., 24 h post-treatment (hpt), [Figure 6B](#) and [Movie S2](#)] showed enhanced green fluorescence in the intracellular phagosomes and reduced cell mobility, likely due to an increased polarization toward the M1 phenotype. However, we did not see significant changes in macrophage numbers at 48 hpw after the treatment with compound 5 ([Figure 6E](#)), which suggests that M1 macrophages may represent a relatively small subpopulation in the tail fin under these experimental conditions. Therefore, we treated wounded larvae with LPS, which leads to a marked increase in TNF- α M1 macrophages in the regenerating fin *in vivo* ([Figure S16](#)). Indeed, whereas most macrophages in 5-treated larvae showed weak green fluorescence and unaffected morphology ([Figure 6C](#)), brighter fluorescence emission was detected in the wound edges of zebrafish treated with LPS and compound 5, with most macrophages showing green fluorescent phagosomes and rounded cellular morphology, characteristic of apoptotic and necrotic cells due to the release of doxorubicin ([Figure 6D](#)).

We further confirmed this observation using TUNEL (terminal deoxynucleotidyl transferase dUTP nick-end labeling) staining, which is used to detect apoptotic cells that undergo extensive DNA degradation, and observed increased apoptosis in zebrafish larvae that had been cotreated with LPS and compound 5 ([Figure S17](#)). Under these conditions, a significant reduction in the macrophage numbers within the regenerating fin was observed when compared to the DMSO control ([Figure 6E](#) and [Figure S18](#)).

Whereas there is experimental evidence that macrophages are required for tail fin regeneration, the exact contribution of specific macrophage subpopulations in the regenerative process is not fully understood. Thus, we measured the regeneration of the tail fin area under different experimental conditions ([Figure 6F](#) and [Figure S19](#)). First, we observed a significant reduction in the regenerated area for 5-treated larvae, suggesting that the depletion of M1 macrophages can impair tissue regeneration. Second, *in vivo* stimulation with LPS, which enhances M1 macrophage polarization, and cotreatment with compound 5 were sufficient to rescue tail fin regeneration to a similar level as the DMSO control. These results are in agreement with the recent observations described by Nguyen-Chi *et al.* in which TNF- α positive M1 macrophages but not TNF- α negative macrophage subpopulations were required for tissue regeneration in zebrafish.⁵¹

CONCLUSIONS

We have developed novel fluorogenic BODIPY–prodrug conjugates targeting proinflammatory subpopulations of macrophages. To the best of our knowledge, these are the first chemical probes able to modulate the function of M1 macrophages *in vivo* without affecting other macrophage subpopulations. Specific cleavage of the prodrug conjugates within the acidic phagosomes of M1 macrophages led to the

intracellular release of a pH-activatable fluorophore as well as the cytotoxic drug doxorubicin for *in situ* cell tracking and subpopulation-specific macrophage depletion. We have demonstrated the applicability of these conjugates *in vivo* using regeneration models to image and deplete phagocytic M1 macrophages. Notably, we have observed a proregenerative role for TNF- α expressing M1 macrophages *in vivo*, which opens new avenues to noninvasively interrogate the contribution of macrophage subpopulations in multiple pathologies without the need for transgenic modifications. This platform will accelerate the development of chemical immunomodulatory agents as subpopulation-specific targeted therapies for immune-related disorders.

EXPERIMENTAL SECTION

General Materials. Commercially available reagents were used without further purification. Thin-layer chromatography was conducted on Merck silica gel 60 F254 sheets and visualized by UV (254 and 365 nm). Silica gel (particle size 35–70 μm) was used for column chromatography. ^1H and ^{13}C spectra were recorded in a Bruker Avance 500 spectrometer (at 500 and 125 MHz, respectively). Data for ^1H NMR spectra are reported as chemical shift δ (ppm), multiplicity, coupling constant (Hz), and integration. Data for ^{13}C NMR spectra are reported as chemical shifts relative to the solvent peak. HPLC–MS analysis was performed on a Waters Alliance 2695 separation module connected to a Waters PDA2996 photodiode array detector and a ZQ Micromass mass spectrometer (ESI-MS) with a Phenomenex column (C_{18} , 5 μm , 4.6×150 mm). Conjugates were purified using a Waters semipreparative HPLC system using a Phenomenex column (C_{18} Axial, 10 μm , 21.2×150 mm) and UV detection.

Chemical Synthesis. BODIPY Ester 3. To a solution of the corresponding BODIPY formamide (**17**, Figure S2) (45 mg, 0.105 mmol) in 6 mL of CHCl_3 under inert atmosphere was added 0.1 mL (0.737 mmol) of DIPEA. The resulting mixture was cooled at 0 $^\circ\text{C}$, and POCl_3 (24 μL , 0.260 mmol) was added dropwise. The reaction mixture was stirred in the cold for 3 h. Then, 10 mL of 2 M NaHCO_3 was added, and the mixture was stirred for 5 min. The aqueous layer was extracted with CH_2Cl_2 (3×20 mL), and the organic extracts were dried over MgSO_4 , filtered, and evaporated under reduced pressure. The resulting isonitrile (**1**) was used without any purification and dissolved in 600 μL of $\text{tBuOH}:\text{CHCl}_3$ (3:2). Formic acid (24 μL , 0.630 mmol), formaldehyde (30% in H_2O , 34 μL , 0.315 mmol), and diethylamine (32 μL , 0.315 mmol) were added. The reaction mixture was stirred for 16 h, and the solvent was removed under reduced pressure to yield a crude residue, which was purified by flash chromatography. Column chromatography in hexane:EtOAc (4:6), synthetic yield 86%. HPLC ($\text{H}_2\text{O}-\text{ACN}$ with 0.1% HCOOH): t_{R} 5.8 min. ^1H NMR (500 MHz, CDCl_3): δ 7.83–7.67 (m, 2H), 7.26 (d, $J = 8.4$ Hz, 2H), 6.03 (d, $J = 14.4$ Hz, 2H), 4.29–4.09 (m, 2H), 3.30 (t, $J = 7.5$ Hz, 2H), 3.21 (br s, 4H), 2.75 (m, 6H), 2.57 (s, 3H), 1.47 (s, 3H), 1.46 (s, 3H), 1.28 (t, $J = 7.1$ Hz, 3H), 1.15 (br s, 6H). MS (m/z): $[\text{M} + \text{H}]^+$ calcd for $\text{C}_{29}\text{H}_{38}\text{BF}_2\text{N}_4\text{O}_3^+$, 539.3; found, 539.3.

BODIPY Ester 4. To a solution of the corresponding BODIPY formamide (**18**, Figure S2) (39 mg, 0.105 mmol) in 6 mL of CHCl_3 under inert atmosphere, was added 1 mL (0.737 mmol) of DIPEA. The resulting mixture was cooled at 0 $^\circ\text{C}$, and POCl_3 (24 μL , 0.260 mmol) was added dropwise. The reaction mixture was stirred in the cold for 3 h. Then, 10 mL of 2 M NaHCO_3 was added, and the mixture was stirred for 5

min. The aqueous layer was extracted with CH_2Cl_2 (3×20 mL), and the organic extracts were dried over MgSO_4 , filtered, and evaporated under reduced pressure. The resulting isonitrile (**2**) was used without any purification and dissolved in 600 μL of $\text{tBuOH}:\text{CHCl}_3$ (3:2). Formic acid (24 μL , 0.630 mmol), formaldehyde (30% in H_2O , 34 μL , 0.315 mmol), and *N*-ethyl glycinate (39 μL , 0.315 mmol) were added. The reaction mixture was stirred for 16 h, and the solvent was removed under reduced pressure to yield a crude residue, which was purified by flash chromatography. Column chromatography in hexane:EtOAc, (1:1), synthetic yield 84%. HPLC ($\text{H}_2\text{O}-\text{ACN}$ with 0.1% HCOOH): t_{R} 7.9 min. ^1H NMR (500 MHz, MeOD): δ 7.88 (d, $J = 8.5$ Hz, 2H), 7.32 (d, $J = 8.5$ Hz, 2H), 6.08 (s, 2H), 3.77 (s, 3H), 3.60 (s, 2H), 3.44 (s, 2H), 2.81 (q, $J = 7.2$ Hz, 2H), 2.50 (s, 6H), 1.49 (s, 6H), 1.14 (t, $J = 7.2$ Hz, 3H). MS (m/z): $[\text{M} + \text{H}]^+$ calcd for $\text{C}_{26}\text{H}_{32}\text{BF}_2\text{N}_4\text{O}_3^+$, 497.2; found, 497.4.

BODIPY Hydrazone 5. N_2 was bubbled through a suspension of doxorubicin (22 mg, 0.038 mmol) and hydrazide BODIPY **22** (Figure S4) (20 mg, 0.038 mmol) in anhydrous MeOH (6 mL) for 30 min. Then TFA (0.5 mL) was added, and the reaction mixture was stirred for 48 h at rt in the dark. Volatiles were removed under reduced pressure, and the resulting residue was purified by semipreparative HPLC to obtain **5** as a red solid, synthetic yield 16%. HPLC ($\text{H}_2\text{O}-\text{ACN}$ with 0.1% HCOOH): t_{R} 5.03 min. ^1H NMR (500 MHz, MeOD): δ 8.54 (s, 1H), 8.08–7.99 (m, 1H), 7.94–7.86 (m, 1H), 7.84 (d, $J = 8.6$ Hz, 2H), 7.66–7.58 (m, 1H), 7.31 (d, $J = 8.6$ Hz, 2H), 6.14 (s, 1H), 6.12 (s, 1H), 5.49 (d, $J = 3.0$ Hz, 2H), 5.21–5.14 (m, 2H), 4.73 (d, $J = 3.1$ Hz, 2H), 4.58 (s, 1H), 4.31 (dt, $J = 7.2$, 6.0 Hz, 1H), 4.07 (s, 3H), 3.99 (s, 1H), 3.70–3.65 (m, 2H), 3.62–3.54 (m, 1H), 3.49–3.44 (m, 2H), 3.37 (d, $J = 3.7$ Hz, 2H), 3.23 (t, $J = 7.7$ Hz, 1H), 3.21–3.16 (m, 1H), 3.17–3.13 (m, 1H), 3.10 (s, 1H), 2.80 (q, $J = 7.1$ Hz, 1H), 2.58 (dd, $J = 8.2$, 7.1 Hz, 1H), 2.51 (s, 3H), 2.39 (dt, $J = 14.8$, 2.2 Hz, 2H), 2.27 (s, 1H), 2.22 (dd, $J = 14.7$, 5.2 Hz, 1H), 2.06 (td, $J = 12.8$, 3.9 Hz, 1H), 1.94–1.87 (m, 1H), 1.50 (s, 3H), 1.49 (s, 3H), 1.41 (d, $J = 6.5$ Hz, 1H), 1.31 (d, $J = 6.6$ Hz, 3H), 1.18 (t, $J = 7.1$ Hz, 6H). HRMS (m/z): $[\text{M}]^+$ calcd for $\text{C}_{54}\text{H}_{62}\text{O}_{12}\text{N}_7\text{BF}_2^+$, 1049.4512; found, 1049.4571.

BODIPY Amide 6. To a solution of doxorubicin hydrochloride (9 mg, 0.015 mmol) and the corresponding BODIPY carboxylic acid **21** (Figure S4) (8 mg, 0.015 mmol) in DMF (0.5 mL) was added DIPEA (8 μL , 0.045 mmol). The solution was stirred for 15 min, and COMU (9 mg, 0.022 mmol) was added predissolved in DMF (0.2 mL). After 6 h stirring at rt, the crude mixture was extracted with CH_2Cl_2 , and the organic extracts were dried over MgSO_4 , filtered, and evaporated under reduced pressure. The mixture was purified by semipreparative HPLC to obtain **6** as a red solid, synthetic yield 16%. HPLC ($\text{H}_2\text{O}-\text{ACN}$ with 0.1% HCOOH): t_{R} 5.9 min. ^1H NMR (500 MHz, $\text{DMSO}-d_6$): δ 10.20 (s, 1H), 7.93 (d, $J = 14.4$ Hz, 1H), 7.84 (d, $J = 8.0$ Hz, 2H), 7.71–7.63 (m, 1H), 7.58–7.49 (m, 1H), 7.30 (d, $J = 8.3$ Hz, 2H), 6.35 (s, 1H), 6.20 (s, 1H), 5.48 (s, 2H), 5.25 (s, 2H), 4.98 (d, $J = 4.9$ Hz, 1H), 4.83 (dt, $J = 9.0$, 6.1 Hz, 2H), 4.62–4.51 (m, 2H), 4.17–4.05 (m, 1H), 3.99 (s, 3H), 3.45–3.34 (m, 2H), 3.18 (d, $J = 5.1$ Hz, 2H), 2.74–2.62 (m, 3H), 2.45–2.33 (m, 3H), 2.30 (s, 3H), 2.25–2.15 (m, 4H), 1.89–1.79 (m, 2H), 1.40 (dd, $J = 7.8$, 3.0 Hz, 2H), 1.38 (s, 6H), 1.17–1.11 (m, 2H), 1.09 (t, $J = 5.4$ Hz, 6H). HRMS (m/z): $[\text{M} + \text{Na}]^+$ calcd for $\text{C}_{54}\text{H}_{60}\text{O}_{13}\text{N}_5\text{BF}_2\text{Na}^+$, 1058.4141; found, 1058.4139.

BODIPY Hydrazone 7. N₂ was bubbled through a suspension of doxorubicin (12 mg, 0.020 mmol) and the corresponding hydrazone BODIPY **20** (Figure S3) (15 mg, 0.030 mmol) in anhydrous MeOH (6 mL) for 30 min. Then TFA (0.5 mL) was added, and the reaction mixture was stirred for 48 h at rt in the dark. Finally, volatiles were removed under reduced pressure, and the resulting residue was purified by semipreparative HPLC to obtain **7** as a red solid, synthetic yield 17%. HPLC (H₂O–ACN with 0.1% HCOOH): *t*_R 5.58 min. ¹H NMR (500 MHz, MeOH-*d*₄): δ 8.57 (s, 1H), 8.04 (dd, *J* = 7.7, 1.1 Hz, 1H), 7.95–7.86 (m, 3H), 7.67–7.60 (m, 1H), 7.31 (d, *J* = 8.7, 2H), 6.08 (s, 2H), 5.49 (d, *J* = 3.8 Hz, 2H), 5.22–5.14 (m, 2H), 4.73 (d, *J* = 3.1 Hz, 2H), 4.31 (q, *J* = 7.0 Hz, 1H), 4.07 (s, 3H), 4.01 (s, 1H), 3.89 (s, 1H), 3.69–3.65 (m, 2H), 3.62–3.44 (m, 1H), 3.40 (s, 1H), 3.37 (s, 1H), 3.21–3.16 (m, 1H), 3.15 (d, *J* = 1.7 Hz, 2H), 3.10 (s, 1H), 3.06 (s, 1H), 2.80 (q, *J* = 7.2 Hz, 1H), 2.51 (s, 3H), 2.49 (s, 3H), 2.43–2.38 (m, 1H), 2.37 (d, *J* = 2.3 Hz, 1H), 2.23 (d, *J* = 5.2 Hz, 1H), 2.20 (d, *J* = 5.2 Hz, 1H), 2.17 (s, 1H), 2.13 (s, 1H), 2.03 (d, *J* = 3.9 Hz, 1H), 1.94–1.88 (m, 1H), 1.49 (s, 6H), 1.31 (d, *J* = 6.6 Hz, 2H), 1.19–1.11 (m, 3H). HRMS (*m/z*): [M + H]⁺ calcd for C₅₂H₅₉O₁₂N₇BF₂⁺, 1022.4277; found, 1022.4258.

BODIPY Amide 8. To a solution of doxorubicin hydrochloride (9 mg, 0.015 mmol) and the corresponding BODIPY carboxylic acid **19** (Figure S3) (7 mg, 0.015 mmol) in DMF (0.5 mL) was added DIPEA (8 μL, 0.045 mmol). The solution was stirred for 15 min, and COMU (9 mg, 0.022 mmol) was added predissolved in DMF (0.2 mL). After 6 h stirring at rt, the crude mixture was extracted with CH₂Cl₂, and the organic extracts were dried over MgSO₄, filtered, and evaporated under reduced pressure. The mixture was purified by semipreparative HPLC to obtain **8** as a red solid, synthetic yield 26%. HPLC (H₂O–ACN with 0.1% HCOOH): *t*_R 6.6 min. ¹H NMR (500 MHz, DMSO-*d*₆): δ 10.43 (s, 1H), 7.94–7.86 (m, 2H), 7.80 (d, *J* = 8.6 Hz, 2H), 7.62 (dd, *J* = 6.6, 3.2 Hz, 1H), 7.26 (d, *J* = 8.5 Hz, 2H), 6.14 (s, 2H), 5.48 (s, 2H), 5.25 (d, *J* = 3.7 Hz, 2H), 4.99–4.93 (m, 1H), 4.83 (dd, *J* = 6.2, 5.1 Hz, 2H), 4.60–4.54 (m, 2H), 4.07–3.97 (m, 1H), 3.95 (s, 3H), 3.57 (s, 2H), 3.49–3.35 (m, 2H), 3.30–3.10 (m, 2H), 2.72–2.60 (m, 3H), 2.45 (s, 6H), 2.39–2.31 (m, 1H), 2.21–2.14 (m, 1H), 1.95–1.77 (m, 1H), 1.51 (dd, *J* = 12.4, 4.5 Hz, 2H), 1.41 (s, 1H), 1.36 (s, 6H), 1.24 (s, 1H), 1.14 (d, *J* = 6.5 Hz, 2H), 1.00 (t, *J* = 7.1 Hz, 3H). HRMS (*m/z*): [M + Na]⁺ calcd for C₅₂H₅₆O₁₃N₅BF₂Na⁺, 1030.3828; found, 1030.3850.

Spectral Characterization of BODIPY–Prodrug Conjugates. Spectroscopic and quantum yield data were recorded on a Synergy HT spectrophotometer (Biotek). Compounds were dissolved at the indicated concentrations, and spectra were recorded at rt. Spectra are represented as means from at least two independent experiments with *n* = 3. Quantum yields were calculated by measuring the integrated emission area of the fluorescence spectra and comparing it to the area measured for fluorescein in basic EtOH as reference (QY: 0.97).⁵²

Cell Culture and Polarization to M1 and M2 Macrophages. RAW264.7 macrophages were grown in DMEM cell culture media supplemented with 10% FBS, antibiotics (100 U mL⁻¹ penicillin, 100 mg mL⁻¹ streptomycin), and 2 mM L-glutamine in a humidified atmosphere at 37 °C with 5% CO₂. For M1 polarization, macrophages were treated with LPS (100 ng mL⁻¹) for 18 h as reported.⁵³ M2 macrophages were isolated upon treatment with IL-4 (100 ng mL⁻¹) for 18 h as reported.⁵⁴ Flow cytometry analysis of M1 and M2 mouse macrophage populations was performed as detailed below using

fluorescent anti-CD86-APC (2 μg mL⁻¹, Biolegend) and anti-CD206-APC antibodies (2 μg mL⁻¹, Biolegend) as M1 and M2 markers, respectively.

For NO production assays, cell supernatants from RAW264.7 macrophages (~90–100% confluence in 24-well plates) that had been polarized or not toward M1 or M2 as described above were collected. NO production was determined using the Griess reagent (Sigma) in which equal volumes (100 μL) of Griess reagent and cell supernatants were mixed and incubated in the dark for 15 min before determining the absorbance at 540 nm in a spectrophotometer.

For arginase activity assays, mouse macrophages were polarized or not toward M1 or M2 as detailed above and the production of urea generated by the arginase-dependent hydrolysis of L-arginine was measured as reported.⁵⁵

Cell Viability. Cell viability was determined using a TACS R MTT Cell Proliferation assay (Trevigen) following the manufacturer's instructions. Briefly, RAW264.7 macrophages were plated on 96-well plates and stimulated as described above when appropriate, reaching 90–95% confluence on the day of the experiment. Compounds were added to the cells at indicated concentrations and incubated at 37 °C overnight. Then cells were washed and treated according to the manufacturer's instructions, and their absorbance values (570 nm) were measured in a Synergy HT spectrophotometer (Biotek). Data analysis was performed using GraphPrism 5.0. Cell viability data was normalized to the proliferation of the cells in cell culture medium.

Cytokine Immunochemical Profiling. Cytokine levels were determined using a Mouse Cytokine Array Panel A (Proteome Profiler, R&D System) following the manufacturer's instructions. Briefly, RAW264.7 macrophages were plated on 12-well plates on the day before the experiment, reaching 70–80% confluence on the day of the experiment. Macrophages were polarized toward the M1 phenotype with LPS (100 ng mL⁻¹) and incubated in the presence or absence of compound **5** (10 μM) at 37 °C for 24 h. Cell supernatants were collected, centrifuged, and treated following the manufacturer's instructions. Membranes were developed in an X-ray Ecomax Processor (Photon Imaging System), scanned, and analyzed using ImageJ.

Flow Cytometry. RAW264.7 macrophages were plated on 24-well plates 4 h before the experiment and incubated at 37 °C. Macrophages were stimulated (with LPS or IL-4), and compounds were added to the cells at the indicated concentrations and incubated at 37 °C for 20 h. Cells were detached, resuspended in CaCl₂ buffer (20 mM HEPES Buffer, 140 mM NaCl, 2 mM CaCl₂, 0.1% BSA), and analyzed by flow cytometry (BD FACSCalibur cytometer, Becton Dickinson) using Annexin V-AF647 (Invitrogen) as the marker for apoptotic cells and/or compound **5** as indicated. Data analysis was performed with the software Flowjo.

Live-Cell Fluorescence Confocal Microscopy. Cells were plated on glass chamber slides Lab-Tek II (Nunc), stimulated with Texas Red conjugated Zymosan A *S. cerevisiae* BioParticles (0.05 mg mL⁻¹), washed with PBS, and incubated with compound **5** (150 nM) at 37 °C. Cells were imaged under a Zeiss LSM510 META fluorescence confocal microscope equipped with a live cell imaging stage. Fluorescence and brightfield images were acquired using a 40× oil objective. Fluorophores were excited with 488 nm (BODIPY) or 543 nm (Texas Red) lasers. All images were analyzed and processed with ImageJ.

Transwell Assays in M1 and M2 Macrophages. RAW264.7 macrophages were plated on 24-well plates equipped with Transwell insert membranes, presoaking the insert in cell growth medium prior to cell seeding overnight. Macrophages were polarized toward M1 (LPS, 100 ng mL⁻¹) or M2 (IL-4, 100 ng mL⁻¹) on separated wells at 37 °C for 24 h. Then, macrophages were washed with PBS and compound 5 (10 μM) was added and incubated in M1/M2 macrophages at 37 °C for 18 h. Macrophages were detached, resuspended in CaCl₂ buffer, and analyzed by flow cytometry using Annexin V-AF647. Data analysis was performed with Flowjo.

Assays in *ex Vivo* Human Monocyte-Derived Macrophages. *Ex vivo* experiments with fresh human peripheral blood from healthy donors were approved by the Accredited Medical Regional Ethics Committee (AMREC, reference number 15-HV-013). Monocytes were obtained by negative isolation from mononuclear cells obtained from whole blood using magnetic beads (pan monocyte isolation kit, Miltenyi) as described elsewhere⁵⁶ and cultured for 7 days in IMDM media with 5% autologous serum. Macrophages were then plated in 96-well plates (40,000 cells/well). Cells were stimulated with LPS (100 ng mL⁻¹), treated with the compounds at indicated concentrations, and incubated at 37 °C overnight to measure their effect in human macrophages as described above. Flow cytometry analysis of M1 human macrophages was performed as detailed above using a fluorescent anti-CD86-APC antibody (2 μg mL⁻¹) (Biolegend).

Total RNA samples from human monocyte-derived macrophages were prepared using RNeasy kits (Qiagen) and reverse transcribed with Quantitect Reverse Transcription kits (Qiagen) following the manufacturer's instructions. cDNA samples were analyzed using a SYBR green based quantitative fluorescence method (Invitrogen) and Kiqstart primers (Sigma). Data was analyzed with β-actin as the housekeeper gene and presented as ΔCT values.

Zebrafish Tissue Regeneration Model. Transgenic macrophage reporter fish Tg(cfms::Gal4-UAS::mCherry) were used to monitor macrophage recruitment in tail fin regeneration assays. A double transgenic Tg(tnfa::eGFP;mpeg1::mCherry) was used to image M1 macrophage polarization *in vivo* upon LPS treatment. For whole-mount TUNEL staining experiments, the transgenic macrophage reporter zebrafish Tg(mfap4::tdTomato-CAAX) were used. Fish were fixed for 2 h in 4% *p*-formaldehyde (PFA) in PBS, permeabilized for 12 h in PBS containing 0.1% Triton X-100 and 3% bovine serum albumin (BSA), and washed in PBS. Zebrafish were stained with the Click-iT TUNEL Alexa 647 Imaging Assay kit (ThermoFisher) following the manufacturer's instructions.

At 2 days post fertilization (dpf), larvae were anesthetized using 0.01% MS222. Tail fins were amputated from the second last section of notochord without damaging the blood vessel using a scalpel. Larvae were then returned to fresh Daneau's solution in a 28.5 °C incubator for 4 h before chemical treatment. Wounded larvae were treated with different compounds in Daneau's solution and then incubated at 28.5 °C at the indicated times and concentrations. Treated larvae were fixed at 48 hpt to quantify macrophage infiltration into regenerating fin. Regeneration was quantified at 72 hpw by measuring the fin area above the cut line, which was identified as a sharp transverse line through the notochord.

***In Vivo* Experiments.** Macrophage number and behavior were monitored during chemical treatment in zebrafish larvae.

Individual larvae were anesthetized in 0.01% MS222 and then mounted on a coverslip in 60 mm glass-bottom dishes using 1% low melting agarose. After immobilization, the dish was filled with Daneau's solution. Live imaging experiments were performed on an inverted Leica SP5 confocal microscope using a 40X water immersion lens. A 594 nm laser was used for excitation of mCherry, and a 488 nm laser was used to excite BODIPY derivatives. Videos were taken at 4 hpw, with 0.5 hpt and 24 hpt. Time-lapse videos were taken at 30 s/frame. All images and videos were analyzed using Volocity 6.0 (PerkinElmer).

■ ASSOCIATED CONTENT

📄 Supporting Information

The Supporting Information is available free of charge on the ACS Publications website at DOI: 10.1021/acscentsci.7b00262.

Full synthetic and characterization details, additional spectral and *in vitro* data, supplementary videos and additional data for *in vivo* fluorescence imaging in zebrafish. (PDF)
Movie S1 (AVI)
Movie S2 (AVI)

■ AUTHOR INFORMATION

Corresponding Authors

*E-mail: yi.feng@ed.ac.uk.

*E-mail: marc.vendrell@ed.ac.uk.

ORCID

Marc Vendrell: 0000-0002-5392-9740

Notes

The authors declare no competing financial interest.

■ ACKNOWLEDGMENTS

A.F. acknowledges a MSCA Individual Fellowship (704912) and funding from the Foundation Alfonso Martin Escudero (FAME, Spain). R.S.-F. acknowledges a MSCA Individual Fellowship (659046). N.B. acknowledges the funding from The EPSRC and MRC Centre for Doctoral Training in Optical Medical Imaging, OPTIMA (EP/L016559/1). Y.F. acknowledges a Wellcome Trust Sir Henry Dale Fellowship (100104/Z/12/Z). M. Vendrell acknowledges funding from the Medical Research Council, the Marie Curie Integration Grant (333847), the Biotechnology and Biological Sciences Research Council (BB/M025160/1), and The Royal Society (RG160289). The authors thank Prof. Ian Dransfield (University of Edinburgh) for helpful discussions and advice and are thankful for the technical support from the Confocal Advanced Light Microscopy (CALM) at the University of Edinburgh.

■ REFERENCES

- (1) Lin, S.-L.; Li, B.; Rao, S.; Yeo, E.-J.; Hudson, T. E.; Nowlin, B. T.; Pei, H.; Chen, L.; Zheng, J. J.; Carroll, T. J.; Pollard, J. W.; McMahon, A. P.; Lang, R. A.; Duffield, J. S. Macrophage Wnt7b is critical for kidney repair and regeneration. *Proc. Natl. Acad. Sci. U. S. A.* **2010**, *107*, 4194–4199.
- (2) Wynn, T. A.; Chawla, A.; Pollard, J. W. Macrophage biology in development, homeostasis and disease. *Nature* **2013**, *496*, 445–455.
- (3) Murray, P. J.; Allen, J. E.; Biswas, S. K.; Fisher, E. A.; Gilroy, D. W.; Goerdt, S.; Gordon, S.; Hamilton, J. A.; Ivashkiv, L. B.; Lawrence, T.; Locati, M.; Mantovani, A.; Martinez, F. O.; Mege, J.-L.; Mosser, D. M.; Natoli, G.; Saeij, J. P.; Schultze, J. L.; Shirey, K. A.; Sica, A.; Suttles, J.; Udalova, I.; van Genderachter, J. A.; Vogel, S. N.; Wynn, T. A.

Macrophage activation and polarization: nomenclature and experimental guidelines. *Immunity* **2014**, *41*, 14–20.

(4) Mosser, D. M.; Edwards, J. P. Exploring the full spectrum of macrophage activation. *Nat. Rev. Immunol.* **2008**, *8*, 958–969.

(5) Forbes, S. J.; Rosenthal, N. Preparing the ground for tissue regeneration: from mechanism to therapy. *Nat. Med.* **2014**, *20*, 857–869.

(6) Minutti, C. M.; Knipper, J. A.; Allen, J. E.; Zaiss, D. M. W. Tissue-specific contribution of macrophages to wound healing. *Semin. Cell Dev. Biol.* **2017**, *61*, 3–11.

(7) Fernandez, A.; Vendrell, M. Smart fluorescent probes for imaging macrophage activity. *Chem. Soc. Rev.* **2016**, *45*, 1182–1196.

(8) De Moliner, F.; Kielland, N.; Lavilla, R.; Vendrell, M. Modern synthetic avenues for the preparation of functional fluorophores. *Angew. Chem., Int. Ed.* **2017**, *56*, 3758–3769.

(9) Weissleder, R.; Nahrendorf, M.; Pittet, M. J. Imaging macrophages with nanoparticles. *Nat. Mater.* **2014**, *13*, 125–138.

(10) Maeda, H.; Kowada, T.; Kikuta, J.; Furuya, M.; Shirazaki, M.; Mizukami, S.; Ishii, M.; Kikuchi, K. Real-time intravital imaging of pH variation associated with osteoclast activity. *Nat. Chem. Biol.* **2016**, *12*, 579–585.

(11) Cobos-Correa, A.; Trojanek, J. B.; Diemer, S.; Mall, M. A.; Schultz, C. Membrane-bound FRET probe visualizes MMP12 activity in pulmonary inflammation. *Nat. Chem. Biol.* **2009**, *5*, 628–630.

(12) Blum, G.; von Degenfeld, G.; Merchant, M. J.; Blau, H. M.; Bogoy, M. Noninvasive optical imaging of cysteine protease activity using fluorescently quenched activity-based probes. *Nat. Chem. Biol.* **2007**, *3*, 668–677.

(13) Oresic Bender, K.; Ofori, L.; van der Linden, W. A.; Mock, E. D.; Datta, G. K.; Chowdhury, S.; Li, H.; Segal, E.; Sanchez Lopez, M.; Ellman, J. A.; Figdor, C. G.; Bogoy, M.; Verdoes, M. Design of a highly selective quenched activity-based probe and its application in dual color imaging studies of cathepsin S activity localization. *J. Am. Chem. Soc.* **2015**, *137*, 4771–4777.

(14) Edgington-Mitchell, L. E.; Bogoy, M.; Verdoes, M. Live cell imaging and profiling of cysteine cathepsin activity using a quenched activity-based probe. *Methods Mol. Biol.* **2017**, *1491*, 145–159.

(15) Yoo, J. S.; Lee, S.-C.; Jow, Z. Y.; Koh, P. Y. X.; Chang, Y.-T. A macrophage-specific fluorescent probe for intraoperative lymph node staging. *Cancer Res.* **2014**, *74*, 44–55.

(16) Yoo, J. S.; Das, R. K.; Jow, Z. Y.; Chang, Y.-T. In vivo detection of macrophage recruitment in hind-limb ischemia using a targeted near-infrared fluorophore. *PLoS One* **2014**, *9*, e103721.

(17) Liu, D.; Yang, F.; Xiong, F.; Gu, N. The smart drug delivery system and its clinical potential. *Theranostics* **2016**, *6*, 1306–1323.

(18) Thapa, P.; Li, M.; Bio, M.; Rajaputra, P.; Nkepang, G.; Sun, Y.; Woo, S.; You, Y. Far-red light-activatable prodrug of paclitaxel for the combined effects of photodynamic therapy and site-specific paclitaxel chemotherapy. *J. Med. Chem.* **2016**, *59*, 3204–3214.

(19) van Dam, G. M.; Themelis, G.; Crane, L. M. A.; Harlaar, N. J.; Pleijhuis, R. G.; Kelder, W.; Sarantopoulos, A.; de Jong, J. S.; Arts, H. J. G.; van der Zee, A. G. J.; Bart, J.; Low, P. S.; Ntziachristos, V. Intraoperative tumor-specific fluorescence imaging in ovarian cancer by folate receptor- α targeting: first in-human results. *Nat. Med.* **2011**, *17*, 1315–1319.

(20) Burggraaf, J.; Kamerling, I. M. C.; Gordon, P. B.; Schrier, L.; de Kam, M. L.; Kales, A. J.; Bendiksen, R.; Indrevoll, B.; Bjerke, R. M.; Moestue, S. A.; Yazdanfar, S.; Langers, A. M. J.; Swaerd-Nordmo, M.; Torheim, G.; Warren, M. V.; Morreau, H.; Voorneveld, P. W.; Buckle, T.; van Leeuwen, F. W. B.; Ødegårdstuen, L. I.; Dalsgaard, G. T.; Healey, A.; Hardwick, J. C. H. Detection of colorectal polyps in humans using an intravenously administered fluorescent peptide targeted against c-Met. *Nat. Med.* **2015**, *21*, 955–961.

(21) Ben-Nun, Y.; Merquioli, E.; Brandis, A.; Turk, B.; Scherz, A.; Blum, G. Photodynamic quenched cathepsin activity based probes for cancer detection and macrophage targeted therapy. *Theranostics* **2015**, *5*, 847–862.

(22) Abd-Elrahman, I.; Kosuge, H.; Wisnes Sadan, T.; Ben-Nun, Y.; Meir, K.; Rubinstein, C.; Bogoy, M.; McConnell, M. V.; Blum, G.

Cathepsin activity-Based probes and inhibitor for preclinical atherosclerosis imaging and macrophage depletion. *PLoS One* **2016**, *11*, e0160522.

(23) Loudet, A.; Burgess, K. BODIPY dyes and their derivatives: syntheses and spectroscopic properties. *Chem. Rev.* **2007**, *107*, 4891–4932.

(24) Kowada, T.; Maeda, H.; Kikuchi, K. BODIPY-based probes for the fluorescence imaging of biomolecules in living cells. *Chem. Soc. Rev.* **2015**, *44*, 4953–4972.

(25) Er, J. C.; Vendrell, M.; Tang, M. K.; Zhai, D.; Chang, Y.-T. Fluorescent dye cocktail for multiplex drug-site mapping on human serum albumin. *ACS Comb. Sci.* **2013**, *15*, 452–457.

(26) Lee, J.-S.; Kim, H. K.; Feng, S.; Vendrell, M.; Chang, Y.-T. Accelerating fluorescent sensor discovery: unbiased screening of a diversity-oriented BODIPY library. *Chem. Commun.* **2011**, *47*, 2339–2341.

(27) Ramirez-Ornelas, D. E.; Alvarado-Martínez, E.; Bañuelos, J.; López Arbeloa, I.; Arbeloa, T.; Mora-Montes, H. M.; Pérez-García, L. A.; Peña-Cabrera, E. FormylBODIPYs: privileged building blocks for multicomponent reactions. The case of the Passerini reaction. *J. Org. Chem.* **2016**, *81*, 2888–2898.

(28) Vázquez-Romero, A.; Kielland, N.; Arévalo, M. J.; Preciado, S.; Mellanby, R. J.; Feng, Y.; Lavilla, R.; Vendrell, M. Multicomponent reactions for de novo synthesis of BODIPY probes: in vivo imaging of phagocytic macrophages. *J. Am. Chem. Soc.* **2013**, *135*, 16018–16021.

(29) Yates, R. M.; Hermetter, A.; Taylor, G. A.; Russell, D. G. Macrophage activation downregulates the degradative capacity of the phagosome. *Traffic* **2007**, *8*, 241–250.

(30) Santra, S.; Kaitanis, C.; Santiesteban, O. J.; Perez, J. M. Cell-specific, activatable, and theranostic prodrug for dual-targeted cancer imaging and therapy. *J. Am. Chem. Soc.* **2011**, *133*, 16680–16688.

(31) Srinivasarao, M.; Galliford, C. V.; Low, P. S. Principles in the design of ligand-targeted cancer therapeutics and imaging agents. *Nat. Rev. Drug Discovery* **2015**, *14*, 203–219.

(32) Maiti, S.; Park, N.; Han, J. H.; Jeon, H. M.; Lee, J. H.; Bhuniya, S.; Kang, C.; Kim, J. S. Gemcitabine-coumarin-biotin conjugates: a target specific theranostic anticancer prodrug. *J. Am. Chem. Soc.* **2013**, *135*, 4567–4572.

(33) Lee, M. H.; Kim, E. J.; Lee, H.; Kim, H. M.; Chang, M. J.; Park, S. Y.; Hong, K. S.; Kim, J. S.; Sessler, J. L. Liposomal texaphyrin theranostics for metastatic liver cancer. *J. Am. Chem. Soc.* **2016**, *138*, 16380–16387.

(34) Liu, D.; Poon, C.; Lu, K.; He, C.; Lin, W. Self-assembled nanoscale coordination polymers with trigger release properties for effective anticancer therapy. *Nat. Commun.* **2014**, *5*, 4182.

(35) Della Rocca, J.; Liu, D.; Lin, W. Nanoscale metal-organic frameworks for biomedical imaging and drug delivery. *Acc. Chem. Res.* **2011**, *44*, 957–968.

(36) Kinchen, J. M.; Ravichandran, K. S. Phagosome maturation: going through the acid test. *Nat. Rev. Mol. Cell Biol.* **2008**, *9*, 781–795.

(37) Canton, J.; Khezri, R.; Glogauer, M.; Grinstein, S. Contrasting phagosome pH regulation and maturation in human M1 and M2 macrophages. *Mol. Biol. Cell* **2014**, *25*, 3330–3341.

(38) Sonawane, S. J.; Kalhapure, R. S.; Govender, T. Hydrazone linkages in pH responsive drug delivery systems. *Eur. J. Pharm. Sci.* **2017**, *99*, 45–65.

(39) Gewirtz, D. A critical evaluation of the mechanisms of action proposed for the antitumor effects of the anthracycline antibiotics adriamycin and daunorubicin. *Biochem. Pharmacol.* **1999**, *57*, 727–741.

(40) Becker, L.; Liu, N. C.; Averill, M. M.; Yuan, W.; Pamir, N.; Peng, Y.; Irwin, A. D.; Fu, X.; Bornfeldt, K. E.; Heinecke, J. W. Unique proteomic signatures distinguish macrophages and dendritic cells. *PLoS One* **2012**, *7*, e33297.

(41) Röszer, T. Understanding the mysterious M2 macrophage through activation markers and effector mechanisms. *Mediators Inflammation* **2015**, *2015*, 816460.

(42) MacMicking, J.; Xie, Q. W.; Nathan, C. Nitric oxide and macrophage function. *Annu. Rev. Immunol.* **1997**, *15*, 323–350.

(43) Jablonski, K. A.; Amici, S. A.; Webb, L. M.; Ruiz-Rosado, J. D.; Popovich, P. G.; Partida-Sanchez, S.; Guerau-de-Arellano, M. Novel markers to delineate murine M1 and M2 macrophages. *PLoS One* **2015**, *10*, e0145342.

(44) Lee, M. H.; Kim, J. Y.; Han, J. H.; Bhuniya, S.; Sessler, J. L.; Kang, C.; Kim, J. S. Direct fluorescence monitoring of the delivery and cellular uptake of a cancer-targeted RGD peptide-appended naphthalimide theragnostic prodrug. *J. Am. Chem. Soc.* **2012**, *134*, 12668–12674.

(45) Haggie, P. M.; Verkman, A. S. Cystic fibrosis transmembrane conductance regulator-independent phagosomal acidification in macrophages. *J. Biol. Chem.* **2007**, *282*, 31422–31428.

(46) Lukacs, G. L.; Rotstein, O. D.; Grinstein, S. Phagosomal acidification is mediated by a vacuolar-type H(+)-ATPase in murine macrophages. *J. Biol. Chem.* **1990**, *265*, 21099–21107.

(47) Buch, T.; Heppner, F. L.; Tertilt, C.; Heinen, T. J. A. J.; Kremer, M.; Wunderlich, F. T.; Jung, S.; Waisman, A. A Cre-inducible diphtheria toxin receptor mediates cell lineage ablation after toxin administration. *Nat. Methods* **2005**, *2*, 419–426.

(48) Zhang, Y.; Choksi, S.; Chen, K.; Pobezinskaya, Y.; Linnoila, I.; Liu, Z. G. ROS play a critical role in the differentiation of alternatively activated macrophages and the occurrence of tumor-associated macrophages. *Cell Res.* **2013**, *23*, 898–914.

(49) Gray, C.; Loynes, C. A.; Whyte, M. K. B.; Crossman, D. C.; Renshaw, S. A.; Chico, T. J. A. Simultaneous intravital imaging of macrophage and neutrophil behaviour during inflammation using a novel transgenic zebrafish. *Thromb. Haemostasis* **2011**, *105*, 811–819.

(50) Wynn, T. A.; Vannella, K. M. Macrophages in tissue repair, regeneration, and fibrosis. *Immunity* **2016**, *44*, 450–462.

(51) Nguyen-Chi, M.; Laplace-Builhe, B.; Travnickova, J.; Luz-Crawford, P.; Tejedor, G.; Lutfalla, G.; Kissa, K.; Jorgensen, C.; Djouad, F. TNF signaling and macrophages govern fin regeneration in zebrafish larvae. *Cell Death Dis.* **2017**, *8*, e2979.

(52) Magde, D.; Wong, R.; Seybold, P. G. Fluorescence quantum yields and their relation to lifetimes of rhodamine 6G and fluorescein in nine solvents: improved absolute standards for quantum yields. *Photochem. Photobiol.* **2002**, *75*, 327–334.

(53) Montana, G.; Lampiasi, N. Substance P induces HO-1 expression in RAW264.7 cells promoting switch towards M2-like macrophages. *PLoS One* **2016**, *11*, e0167420.

(54) Chen, Y.; Liu, W.; Wang, Y.; Zhang, L.; Wei, J.; Zhang, X.; He, F.; Zhang, L. Casein kinase 2 interacting protein-1 regulates M1 and M2 inflammatory macrophage polarization. *Cell. Signalling* **2017**, *33*, 107–121.

(55) Corraliza, I. M.; Campo, M. L.; Soler, G.; Modolell, M. Determination of arginase activity in macrophages: a micromethod. *J. Immunol. Methods* **1994**, *174*, 231–235.

(56) Hart, S. P.; Rossi, A. G.; Haslett, C.; Dransfield, I. Characterization of the effects of cross-linking of macrophage CD44 associated with increased phagocytosis of apoptotic PMN. *PLoS One* **2012**, *7*, e33142.